nature materials

REVIEW ARTICLE

PUBLISHED ONLINE: 22 MAY 2013 | DOI: 10.1038/NMAT3585

Single spins in self-assembled quantum dots

Richard J. Warburton

Self-assembled quantum dots have excellent photonic properties. For instance, a single quantum dot is a high-brightness, narrow-linewidth source of single photons. Furthermore, the environment of a single quantum dot can be tailored relatively easily using semiconductor heterostructure and post-growth processing techniques, enabling electrical control of the quantum dot charge and control over the photonic modes with which the quantum dot interacts. A single electron or hole trapped inside a quantum dot has spintronics applications. Although the spin dephasing is rather rapid, a single spin can be manipulated using optical techniques on subnanosecond timescales. Optical experiments are also providing new insights into old issues, such as the central spin problem. This Review provides a snapshot of this active field, with some indications for the future. It covers the basic materials and optical properties of single quantum dots, techniques for initializing, manipulating and reading out single spin qubits, and the mechanisms that limit the electron-spin and hole-spin coherence.

The superposition principle is at the heart of quantum mechanics: a spin, for instance, can simultaneously be in the 'up' and 'down' states. As a consequence, two spins can be entangled, the entanglement representing an intimate link even though the spins may be far apart. Exploring these concepts experimentally is challenging as it is difficult to shield the quantum system from the deleterious effects of the environment. Most of the early successes involving light quanta (photons) were made in the context of atomic physics. However, a quiet revolution has taken place in the past decade or so: materials advances in both semiconductors and diamond have enabled experiments to be performed in the solid state with single spins and single photons. As semiconductors are so important for real-world devices, these experiments may lead to applications. In particular, a qubit in a semiconductor has potential applications in the areas of quantum metrology, quantum communication and quantum information processing.

A qubit is a two-level quantum system that can be initialized, manipulated and read out. The manipulation in particular should be predictable: it should be carried out before the qubit loses information encoded in its phase, an issue known as the decoherence problem. Implementing the qubit concept in a semiconductor leads naturally to the electron spin[1], which is a natural two-level system. An electron spin interacts only weakly (through the spin–orbit interaction) with the main source of decoherence in bulk semiconductors, the lattice vibrations (phonons)[2], and has a strong interaction with experimental probes (unlike a nuclear spin for instance). The search for a coherent electron spin in the solid state has led most spectacularly to the nitrogen–vacancy centre in diamond. The atomic-like confinement, along with the low-mass carbon atoms, suppresses the spin–orbit interaction. Furthermore, spin dephasing arising from spin noise in the host nuclear spins is small and can be suppressed even further with isotopically pure material such that the spin coherence time can reach a millisecond even at room temperature[3]. However, it is challenging to process diamond into a real device. Conversely, inorganic semiconductors have very attractive and flexible materials properties. The ability to design and realize semiconductor heterostructures along with sophisticated post-growth processing has led to devices such as high-frequency transistors and semiconductor lasers with excellent performance. Can spin coherence be achieved not just in diamond but also in group III–V semiconductors?

The physics is dominated by investigations into decoherence, the interaction of the spin with the environment[4]. To suppress the interaction with the phonons, an electron spin should be confined to a quantum dot, a nanoscale potential trap. In this case, there is a large mismatch between the extent of the electron wavefunction and the typical phonon wavelength at low temperature, thus suppressing the electron–phonon interaction. A quantum dot can be defined by depleting locally a two-dimensional electron gas with nanofabricated gate electrodes[5]. The quantization energy is typically small, a few meV, and the devices must therefore be operated at subkelvin temperatures. Spectacular success has been achieved using this approach[6]. An alternative is to fabricate a layer of quantum dots during the semiconductor layer-by-layer growth. These self-assembled quantum dots are just a few tens of nanometres across such that the quantization energy is large (of the order of tens of meV) and a lot of spin experiments can be carried out at liquid helium temperature (4 K). Furthermore, a self-assembled quantum dot in a direct-bandgap host such as gallium arsenide has a strong optical transition across the main gap of the semiconductor. On the one hand, the large optical dipole moment allows the spin to be initialized, manipulated and read out all with optical techniques[7]. On the other hand, the link between single spins and single photons opens up applications in quantum communication. Significantly, the materials developments that are so crucial for advanced semiconductor lasers (semiconductor Bragg mirrors, controlled doping, post-growth etching and contacting) can all be exploited to enhance and control the optical properties. The tantalizing prospect is that even if the spin coherence times are modest by atomic-physics standards, spin rotations can be accomplished on subnanosecond timescales, allowing many gate operations before coherence is lost.

This Review describes some spin experiments on self-assembled quantum dots, focusing on single quantum dot experiments with resonant optical excitation. It makes no attempt to be complete. Instead, the aims are to introduce the main concepts, to provide a snapshot of the present status in the field and to point to some future prospects.

Self-assembled quantum dots

A simplified introduction to self-assembled quantum dots is provided.

Department of Physics, University of Basel, Klingelbergstrasse 82, CH-4056 Basel, Switzerland.
e-mail: richard.warburton@unibas.ch

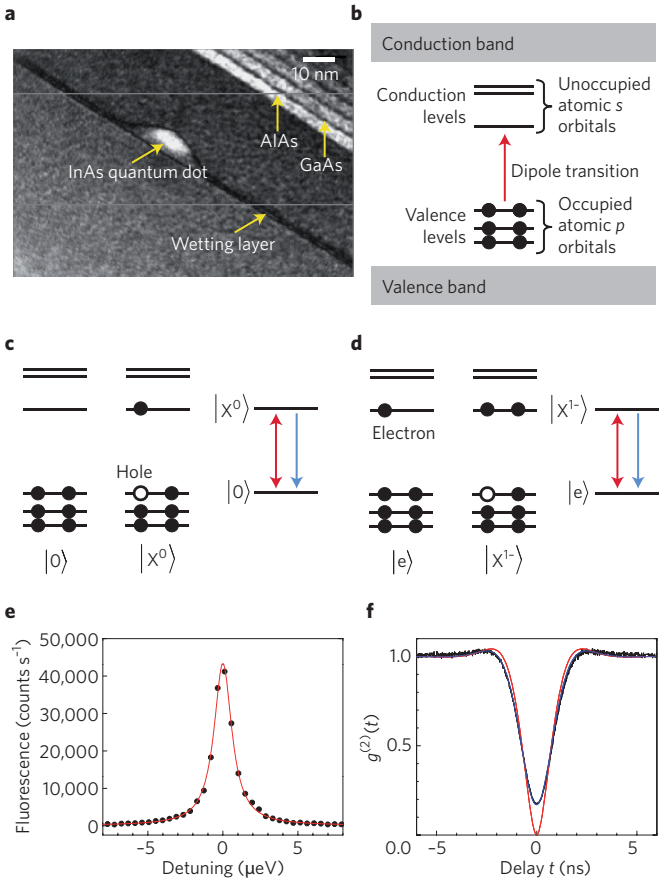

Figure 1 | Photonics of a single self-assembled quantum dot at zero magnetic field. a, Transmission electron microscopy image showing an InAs quantum dot with its associated wetting layer, embedded in GaAs and capped with an AlAs/GaAs superlattice. **b**, The energy level structure of a self-assembled quantum dot. There are discrete, atom-like conduction and valence levels. At higher energies, there are the conduction and valence energy bands associated with the two-dimensional wetting layer (and bulk GaAs at higher energy still). A strong optical dipole transition connects the highest-energy valence level with the lowest-energy conduction level. **c**, The vacuum state $|0\rangle$ and the optically excited state $|X^0\rangle$ are represented as the ground and excited state of a two-level atom (red arrow represents the optical coupling, blue arrow spontaneous emission). The $|X^0\rangle$ state is an exciton, an electron–hole pair. **d**, A quantum dot can be loaded with a single excess electron (see Fig. 3). In this case, the ground state is $|e\rangle$ and the optically excited state $|X^{1-}\rangle$ consisting of two electrons (in a singlet) and a hole. **e**, Laser spectroscopy on a single quantum dot at a wavelength close to 950 nm at a temperature of 4.2 K. The resonance fluorescence is plotted as a function of laser detuning. The linewidth is 1.6 μeV (400 MHz). The signal corresponds to the count rate on a silicon avalanche photodiode. **f**, The intensity correlation coefficient $g^{(2)}(t)$ of the resonance fluorescence measured with a Hanbury Brown–Twiss interferometer (black line). The dip at zero delay shows clear photon antibunching. The signal at zero delay is dominated by the jitter of the detector (0.5 ns); the slight overshoot at delay ~1 ns is the first hint of a Rabi oscillation that becomes marked at higher laser power. The blue line is a convolution of the two-level atom $g^{(2)}(t)$ with the response of the detectors; the red line is the two-level atom $g^{(2)}(t)$ alone. Panel **a** courtesy of Jean-Michel Chauveau, Arne Ludwig, Dirk Reuter and Andreas Wieck. Data in panels **e**,**f** courtesy of Andreas Kuhlmann, Julien Houel and Arne Ludwig.

Quantum dot self-assembly. The self-assembly of a quantum dot during growth is driven by strain. The workhorse system for optical experiments is indium arsenide (InAs) on gallium arsenide (GaAs). InAs has a 7% larger lattice constant than GaAs: InAs grows on GaAs initially layer-by-layer, but after just 1.5 monolayers InAs quantum dots form[8]. The quantum dots are subsequently capped by GaAs and are generally embedded into a semiconductor heterostructure (Fig. 1a). Typically, the quantum dots are ~5 nm high with a diameter of ~20 nm and are therefore smaller than those produced by lithography. The nanoscale confinement leads to a few discrete conduction levels separated by ~20–50 meV, and a few discrete valence levels separated by ~10–25 meV (Fig. 1b). The details are complex however: InAs dots are highly alloyed with Ga, the In composition rises from bottom to top[9] and the details depend on the exact growth procedure. The total number of atoms in such a quantum dot is ~10^5.

Optical properties of a single self-assembled quantum dot. An InGaAs/GaAs quantum dot has a strong optical transition between the highest valence level and the lowest conduction level[10] (Fig. 1b). In semiconductor language, optical excitation creates an exciton, an electron–hole pair (Fig. 1c,d). For as-grown InGaAs/GaAs quantum dots, the optical transition lies at an inconvenient wavelength, ~1,200 nm at low temperature, but can be blue-shifted by thermal annealing, which encourages alloying of InAs and GaAs. The optical transition post-annealing can be engineered to lie anywhere between 900 and 1,200 nm. Many experiments are carried out around 950 nm, a wavelength at which both good lasers and detectors are available. The annealing can take place either during growth[11] or through post-growth annealing[12]. The radiative lifetime is short, typically ~0.8 ns (ref. 13), corresponding to a dipole moment of 0.6 nm × e, where e is the electronic charge[14].

Based on this optical transition, a single self-assembled quantum dot is a robust, fast, narrow-linewidth source of on-demand photons, properties not shared by any other emitter. The traditional problem of extracting the photons out of the high-index host material (GaAs has a refractive index of 3.5) can be solved by also engineering the photonic states. For instance, by embedding the quantum dots in a GaAs waveguide, and using a taper as an out-coupler, high-fidelity single-photon emission with a quantum efficiency as high as ~70% has been achieved[15].

Many optical experiments in this field rely on non-resonant excitation in which a high-energy continuum (Fig. 1b) is occupied with electron–hole pairs. The electron and hole levels in the quantum dot are populated by fast relaxation, and the spontaneous emission on exciton decay (the photoluminescence) can be detected. An example is shown in Fig. 2b. This is a relatively simple experiment but lacks the power of true laser-spectroscopy methods that involve driving the optical resonance with a coherent laser (Fig. 1c,d). The interaction of a single quantum dot with a coherent laser tuned to the optical resonance was initially detected through a change in the transmission coefficient, a 'ΔT experiment'[16]. Meanwhile, the resonance fluorescence can also be detected, discriminating between resonance fluorescence and scattered laser light with a dark-field technique based either on the propagation direction[17] or on the polarization[8,19] (Fig. 1e). Remarkably, all the features of a driven two-level system known from atomic physics have been observed on a single quantum dot. These include a Lorentzian absorption lineshape[16] (Fig. 1e); power broadening and power-induced transparency[20]; the dynamic Stark effect[21]; Rabi oscillations[17], the Mollow triplet and antibunching of resonance fluorescence[17] (Fig. 1f). Routinely, close-to-transform limited optical transitions are observed in laser spectroscopy experiments on single InGaAs/GaAs quantum dots[22]. (A significant part of the residual linewidth at low Rabi couplings arises from a spectral fluctuation arising from electrical noise in the semiconductor that shifts the optical transition energy through the Stark effect[16,22]; at higher Rabi couplings, phonon-induced exciton decoherence is observed[23].)

The vacuum state (empty quantum dot) and the exciton state X^0 (electron–hole complex) can form the two logical states $|0\rangle$ and

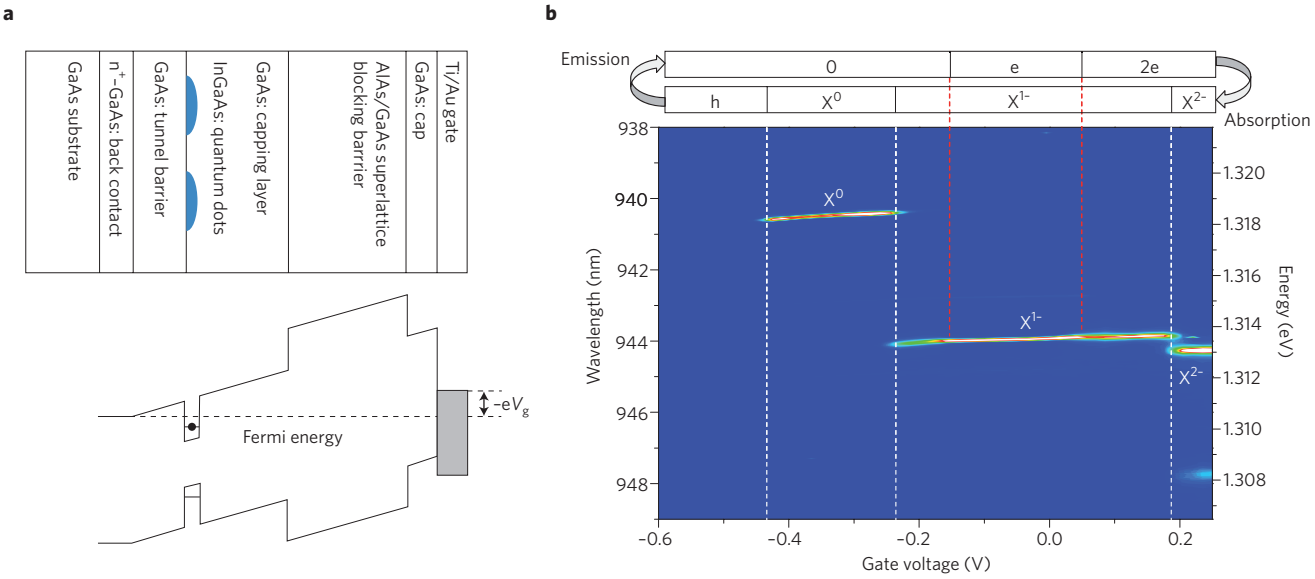

Figure 2 | Coulomb blockade of a single quantum dot. a, Layer structure of a typical heterostructure for experiments controlling the charge state of a quantum dot (top). A layer of self-assembled quantum dots is embedded in a vertical tunnelling structure. The quantum dots are in tunnel contact with the Fermi sea in the n^+ layer; the blocking barrier prevents current flow to the surface; a Schottky gate on the surface allows control of the vertical electric field. Typically, the tunnel barrier (GaAs) is 12–40 nm thick, the capping layer 10–150 nm thick, blocking barrier >100 nm thick and the Schottky gate is a semi-transparent metal layer, for example, 5–10 nm of Ti/Au. A voltage applied to the gate, V_g, tunes the energy of the first confined electron level relative to the Fermi energy as shown schematically in the band diagram (bottom). At low temperature and large electric field, the quantum dot conduction level lies above the Fermi energy and is therefore unoccupied; when the conduction level lies below the Fermi energy but close to it (shown), the conduction level is singly occupied (shown); at more positive V_g it is doubly occupied. **b**, The photoluminescence from a single quantum dot in a vertical tunnelling structure is shown as a function of V_g at a temperature of 4.2 K. The steps in the photoluminescence energy correspond to charging events. X^0 refers to the neutral exciton (an electron–hole pair); X^{1-} to the negatively charged trion (a two electron–one hole complex); X^{2-} the doubly charged exciton (a three electron–one hole complex). Note that the charging event without a hole, $|0\rangle \rightarrow |e\rangle$, takes place at slightly more positive V_g than the charging event with a hole, $|X^0\rangle \rightarrow |X^{1-}\rangle$, on account of the Coulomb energies: the electron–hole on-site Coulomb energy is larger than the electron-electron on-site Coulomb energy. Conversely, the $|e\rangle \rightarrow |2e\rangle$ charging event takes place at more negative V_g than the $|X^{1-}\rangle \rightarrow |X^{2-}\rangle$ charging event as the X^{2-} state has a total of three electrons, the 'third' forced to occupy the first excited conduction level by the Pauli principle. The main features in the photoluminescence characterization correspond to charging events in the initial state, the exciton state (white dashed lines). However, charging events in the final state are revealed by hybridization effects in the X^{1-} plateau (red dashed lines)[102]. Probing a single spin with resonant laser excitation involves working in the V_g window defined by the two dashed red lines. Experimental data in panel **b** provided courtesy of Paul Dalgarno.

$|1\rangle$ of a qubit: the set of laser spectroscopy experiments can be described in terms of exciton qubit initialization, manipulation and readout. However, spontaneous emission from X^0 to the ground state represents a fast decoherence process. Experiments exploiting quantum coherence of the exciton qubit are therefore limited to the domain of ultrafast optics. A single spin can also be manipulated with ultrafast laser techniques but potentially retains its quantum coherence over much longer timescales. This is a key motivating factor for developing a spin qubit in an optically active quantum dot.

The electron spin

Techniques to manipulate the spin of an electron trapped in a self-assembled quantum dot are discussed, along with the dephasing and decoherence mechanisms.

Singly charged self-assembled quantum dots. Implementing the concept of a spin qubit with a self-assembled quantum dot involves trapping a single electron or hole. This can be achieved by including a doped layer close to the quantum dot layer in the growth process, such that some of the quantum dots are permanently occupied with an excess electron[24] or hole[25] at low temperature. A more flexible technique allowing for considerable *in situ* tuning is to embed the quantum dot layer in a vertical tunnelling device[26,27] (Fig. 2). The device operates in the Coulomb blockade regime that at 4 K is highly pronounced based on the huge on-site Coulomb energy-to-thermal energy ratio (~25 meV:0.4 meV). The Coulomb blockade is revealed by clear steps in the photoluminescence energy from a single quantum dot[27] (Fig. 2b). A single electron is trapped in the quantum dot over a Coulomb blockade plateau (Fig. 2b): a voltage chosen within this region allows access to single-spin physics[28]. In the Coulomb blockade regime, tunnelling is suppressed to first order but the second-order process, co-tunnelling, survives[29]. Co-tunnelling represents a spin-relaxation mechanism: the quantum dot electron spin is swapped with the spin of an electron close to the Fermi energy in the Fermi sea of the n^+ layer. A convenient property of the vertical tunnelling structure is that the co-tunnelling rate can be tuned electrically over several orders of magnitude from rapid at the edge of the plateau to slow in the plateau centre[29–33].

Optics of a singly charged self-assembled quantum dot. In a magnetic field along the growth direction z, the electron spin eigenstates, $|\uparrow\rangle_z$ and $|\downarrow\rangle_z$, are split by the Zeeman effect (Fig. 3a). The optically excited eigenstates are the trion states (the X^{1-} states) consisting of two spin-paired electrons and a lone hole spin, $|\uparrow\downarrow, \Uparrow\rangle_z$ and $|\uparrow\downarrow, \Downarrow\rangle_z$. In the effective mass description, the so-called **k·p** model, the hole state is constructed from heavy-hole (J, $J_z = 3/2, \pm 3/2$), light-hole (J, $J_z = 3/2, \pm 1/2$), spin–orbit split-off (J, $J_z = 1/2, \pm 1/2$) and electron (S, $S_z = 1/2, \pm 1/2$) Bloch states, but the heavy-hole contribution is dominant on account of both strong vertical confinement and in-built non-hydrostatic strain (both of which reduce the light-hole component), and the large fundamental gap and the spin–orbit interaction (which limit the admixture of the conduction

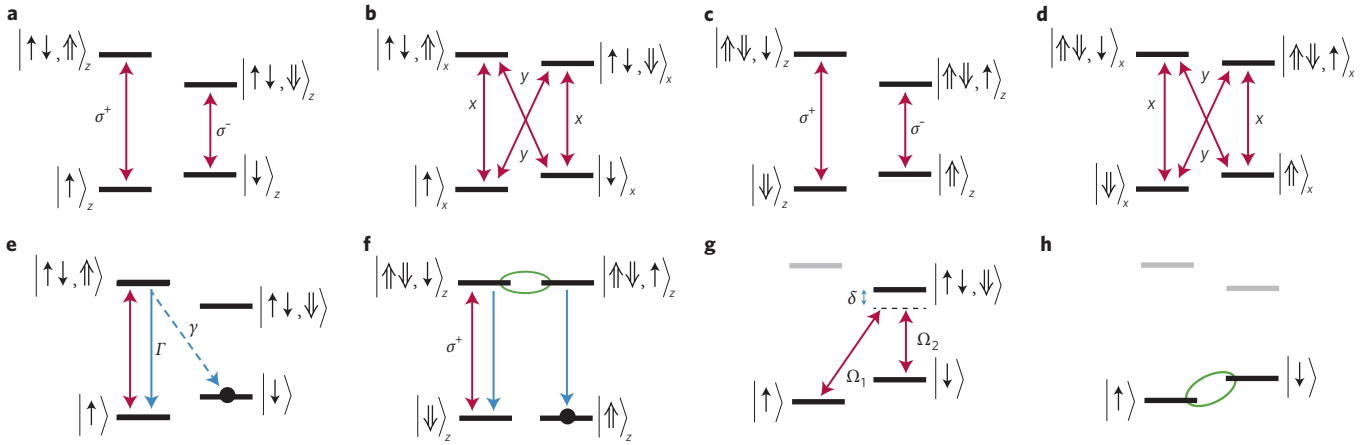

Figure 3 | Single spin physics and level diagrams. a, The electron spin states, $|\uparrow\rangle_z$ and $|\downarrow\rangle_z$, split by the Zeeman effect in an external magnetic field **B** along the growth *z*-direction. The electron *g*-factor is typically small and negative (g~−0.5; Zeeman splitting −30 μeV T^{-1}). Optical excitation forms the X^{1-} trion states, $|\uparrow\downarrow, \Uparrow\rangle_z$ and $|\uparrow\downarrow, \Downarrow\rangle_z$, consisting of two spin-paired electrons and a hole, split by the hole Zeeman effect (Zeeman splitting ~70 μeV T^{-1}). For a pure heavy-hole state, the red arrows show the transitions allowed by the conservation of angular momentum (right-handed polarization σ^+: spin +1; left-handed polarization σ^-: spin −1). **b**, For **B** along *x* , both vertical and diagonal transitions are allowed. Expanding the *x*-basis eigenstates in the *z*-basis shows that the vertical transitions are driven with *x* linearly polarized light; the diagonal transitions with *y* linearly polarized light. The electron Zeeman energy is essentially the same as in **a** but the hole Zeeman energy is considerably smaller. **c**, The hole spin states, $|\Downarrow\rangle_z$ and $|\Uparrow\rangle_z$, split by the Zeeman effect in **B** along *z*, showing the allowed transitions. **d**, Level diagram for a hole spin with **B** along *x*. **e**, Electron spin initialization via optical pumping. The allowed transition, $|\uparrow\rangle \leftrightarrow |\uparrow\downarrow, \Uparrow\rangle$, is driven with a narrowband laser. Spontaneous emission takes place at rate Γ from the vertical transition $|\uparrow\downarrow, \Uparrow\rangle \rightarrow |\uparrow\rangle$ and at rate γ from the diagonal transition $|\uparrow\downarrow, \Uparrow\rangle \rightarrow |\downarrow\rangle$. Provided the optical coupling is comparable to Γ and γ is much greater than the spin relaxation rate, the electron is shelved by the diagonal spontaneous emission in the $|\downarrow\rangle$ state. With **B** along *x*, $\gamma = \Gamma$ and spin initialization takes about a nanosecond[48]. With **B** along *z*, $\gamma << \Gamma$ as the diagonal transition is forbidden (weakly allowed either by a nuclei-induced tilt of the quantization axis or by heavy hole–light hole mixing) and spin initialization takes longer, about a microsecond[47]. **f**, Optical pumping of a single hole spin at **B** = 0. The allowed transition $|\Downarrow\rangle_z \leftrightarrow |\Uparrow\Downarrow, \downarrow\rangle_z$ is driven with σ^+-polarization. The $|\Uparrow\Downarrow, \downarrow\rangle_z$ and $|\Uparrow\Downarrow, \uparrow\rangle_z$ states are coupled (green line) via the small in-plane magnetic field generated by the nuclear spins. Spontaneous emission from the $|\Uparrow\Downarrow, \uparrow\rangle_z$ state occupies the $|\Uparrow\rangle_z$ state that is shielded from the laser by the selection rules. **g**, An optical Λ-system in an in-plane **B**. The two ground states are the electron spin states; the common upper level one of the exciton states. The two arms of the Λ-system are driven with two lasers, pump and probe, Rabi energies $\hbar\Omega_1$ and $h\Omega_2$. At the two-photon resonance (frequency difference of the lasers equals the splitting of the ground states), one of the three eigenstates is an admixture purely of $|\uparrow\rangle$ and $|\downarrow\rangle$, the dark state[36], revealed by a dip in the probe absorption, coherent population trapping. **h**, In the limit $\delta >> \Omega_1, \Omega_2$, one approximate eigenstate is the upper state alone and the optical couplings represent an effective coupling (green line) $\Omega_1\Omega_2/2\delta$ between the two spin states[7]. With laser pulses, this effective $|\uparrow\rangle \leftrightarrow |\downarrow\rangle$ coupling can be turned rapidly on and off. The grey levels are those that exist but remain unpopulated.

and spin–orbit split-off Bloch states, respectively). In the idealized limit where the hole states $|\Uparrow\rangle_z$ and $|\Downarrow\rangle_z$ have a pure heavy-hole character, the optical selection rules are particularly simple (as shown in Fig. 3a):

$$|\uparrow\rangle_z \xleftrightarrow{\sigma^+} |\uparrow\downarrow, \Uparrow\rangle_z$$
$$|\downarrow\rangle_z \xleftrightarrow{\sigma^-} |\uparrow\downarrow, \Downarrow\rangle_z$$

Experiments have demonstrated that these selection rules are 'almost hard'[34,35]. The 'diagonal transitions', $|\uparrow\rangle_z \leftrightarrow |\uparrow\downarrow, \Downarrow\rangle_z$ and $|\downarrow\rangle_z \leftrightarrow |\uparrow\downarrow, \Uparrow\rangle_z$, are weakly allowed through the light-hole component of the hole spin states. The case of a hole spin in the *z*-basis is shown in Fig. 3c. In this case, the exciton states consist of two spin-paired holes and a lone electron spin.

In a magnetic field in the growth plane, the *x*-direction say, the spin eigenstates in the *x*-basis are admixtures of eigenstates in the *z*-direction. Applying the *z*-selection rule to this geometry results in a new level diagram: all four transitions among the four levels are now allowed, each equally strong. The 'vertical' transitions are driven with *x*-polarized laser light, and the diagonal transitions with *y*-polarized laser light, as shown in Fig. 3b for an electron spin and Fig. 3d for a hole spin. Significantly, once the exciton levels are well separated, two optical Λ-systems can be established: the two qubit states, $|\uparrow\rangle$ and $|\downarrow\rangle$ or $|\Uparrow\rangle$ and $|\Downarrow\rangle$, are coupled to a common upper level (Fig. 3g). This allows coherent population trapping in a spectroscopy experiment[36–38] (Fig. 3g) and spin rotation by a laser pulse[39–42] (Fig. 3h).

Electron spin initialization. The electron spin can be initialized with close-to-100% fidelity by optical pumping[30,43]. With a magnetic field in the *z*-direction (Fig. 4a) it was discovered that the contrast in a ΔT-experiment disappears on driving one of the allowed transitions[30] (Fig. 4b,c). The interpretation is that driving the $|\uparrow\rangle \leftrightarrow |\uparrow\downarrow, \Uparrow\rangle$ transition 'pumps' the population into the $|\downarrow\rangle$ state by weakly allowed spontaneous emission $|\uparrow\downarrow, \Uparrow\rangle \rightarrow |\downarrow\rangle$. Once the spin is 'shelved' in the $|\downarrow\rangle$ state, it no longer interacts with the laser on account of both the laser's polarization and frequency. This interpretation is given stunning confirmation by driving both allowed transitions simultaneously, which restores the contrast in the ΔT-signal[30] (Fig. 4d). The experiment is sensitive to the spin-relaxation time, T_1 (ref. 31). At low magnetic fields, below about 0.3 T, spin pumping is ineffective as T_1 is too short: an electron spin can undergo a spin-flip with a nuclear spin through the contact part of the hyperfine interaction[44]. At larger magnetic fields, the electron–nuclear spin-flip rate is suppressed on account of energy conservation — the electron gyromagnetic ratio is approximately 10^3 times larger than the nuclear gyromagnetic ratio — and at fields of about 1 T, T_1 can reach a remarkably large value of about a second[31,45]. At high fields, T_1 is smaller and has a B^{-5}-dependence[46], signifying spin relaxation by means of phonons[2]. The mechanism responsible for the small but finite optical dipole of the 'forbidden' diagonal transitions can also be determined through the magnetic field dependence of the spin pumping time, the time required to drive the system from a statistical mixture of the $|\uparrow\rangle$ and $|\downarrow\rangle$ states into the steady state, either $|\uparrow\rangle$ or $|\downarrow\rangle$. At low magnetic fields, the nuclear spins are responsible (they rotate the quantization axis away from the applied

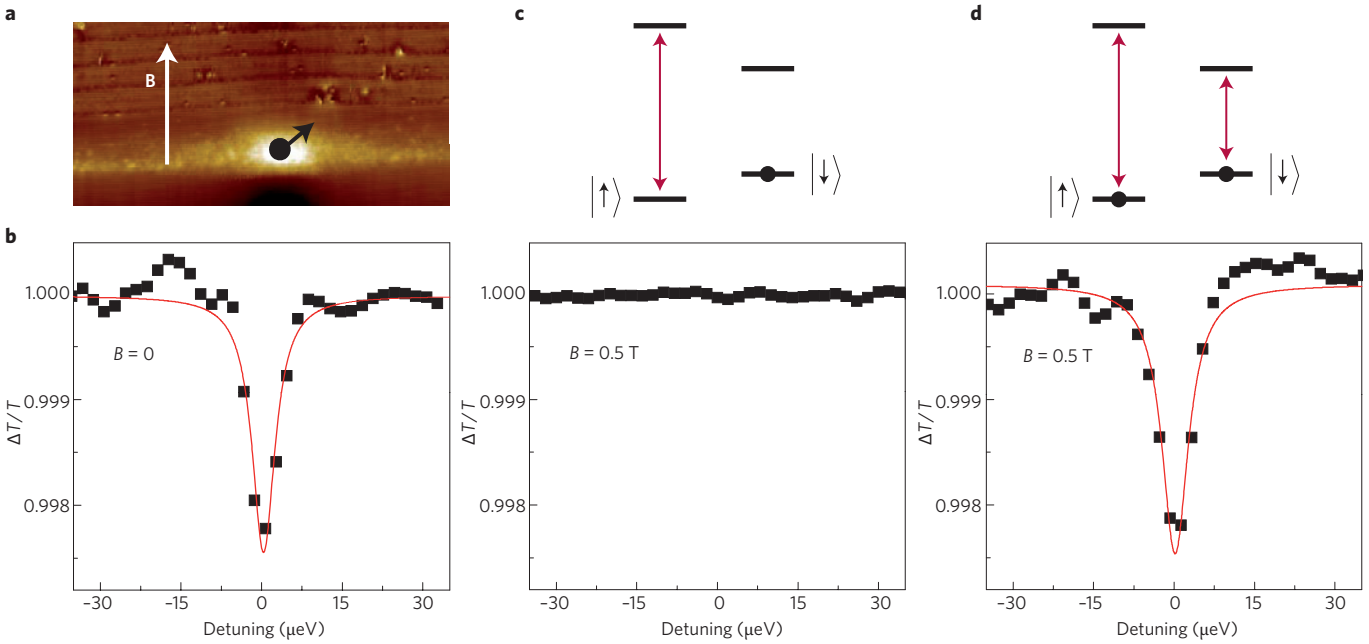

Figure 4 | Electron spin initialization and manipulation. Electron spin initialization with a magnetic field along the *z*-direction at 4.2 K. **a**, A cross-sectional scanning tunnelling microscope image shows an InGaAs quantum dot, 80 × 40 nm^2. **b**, At $B = 0$, the quantum dot (occupied with a single electron) shows a clear transmission dip (laser spectroscopy with a narrowband laser at 4.2 K). **c**, The transmission dip disappears at $B = 0.5$ T on account of optical pumping: the electron is shelved in the $|\downarrow\rangle$ state. The small magnetic field strongly suppresses the electron-spin relaxation process through a flip-flop with a nuclear spin. **d**, The transmission dip reappears with a re-pump laser, that is, on driving both optical transitions simultaneously. Electron spin initialization by means of optical pumping was first achieved by Mete Atatüre in the group of Atac Imamoğlu[30]; this data was recorded by Martin Kroner in the course of two-colour laser spectroscopy experiments[43]. The red curves are Lorentzian fits to the data. Panel **a** courtesy of Paul Koenraad.

field direction); at large magnetic fields, the light hole part of the upper state dominates[47].

With a magnetic field in the *z*-direction, the spin initialization time is as large as a microsecond on account of the weak diagonal transitions: about 10^3 cycles of the allowed transition are required before diagonal spontaneous emission initializes the spin[47] (Fig. 3e). The initialization time is reduced to just a nanosecond with a field in the (x,y)-plane[48]. In this case, the diagonal transition is equally strong as the vertical transition (Fig. 3b). Fast initialization is achieved at the slight expense of fidelity: the pumped spin is shielded from the initialization laser on account of the laser's frequency only.

Electron spin manipulation. The optical transition across the fundamental gap enables fast spin manipulation[7]. The key is to establish an optical Λ-system with an in-plane magnetic field[37,48] (Fig. 3g). A 'Raman transition' provides an effective coupling between the two ground states, $|\uparrow\rangle$ and $|\downarrow\rangle$ (Fig. 3h), when both transitions are driven with highly and equally detuned lasers: a photon is transferred by the quantum dot from one laser field to the other. When the detuning is much larger than the Zeeman energies, a single circularly polarized laser drives all four optical resonances, and both Λ-systems contribute to the effective coupling[39,40].

Following spin initialization, a spin rotation can be driven by a detuned laser pulse, and the spin readout by detecting the fluorescence induced by the initialization laser[39,40] (Fig. 5). Rabi flopping between the two spin states can be achieved on a sub-10 ps timescale (Fig. 5d). This illustrates the power of the optical approach: spin rotations can be achieved on very short timescales, Rabi flopping times that are at present inaccessible with techniques based on high-frequency electronics.

Manipulating a single spin is also possible with an alternating magnetic field[49], the traditional approach in electron spin resonance. Optically detected single-spin resonance has been demonstrated in a continuous-wave spectroscopy experiment using an a.c. magnetic field generated by an oscillating current in a nearby loop, generating fields of B_{ac} ~10 μT (ref. 50). The ΔT-signal is quenched by spin pumping but reappears at the spin resonance. This optical detection is attractive because of the in-built amplification: absorption of a microwave photon triggers the absorption of an optical photon at a frequency 10^5 times larger[51]. However, spin rotations are likely to be slow unless B_{ac} is significantly increased. An alternative is to drive the spin resonance electrically with an a.c. electric field rather than with an a.c. magnetic field — a spatial translation of the electron wavefunction mimics an a.c. magnetic field through the spin–orbit interaction[52,53] — but this concept has yet to be applied to a self-assembled quantum dot.

Electron spin coherence. The time-averaged electron-spin coherence time, the dephasing time T_2^*, has been measured in both the frequency domain with a coherent population trapping experiment and in the time domain with a driven spin experiment. The experiments yield a disappointingly small T_2^*, just a few nanoseconds[24,37,40], many orders of magnitude less than the spin relaxation time, T_1. The origin of the fast dephasing is noise in the nuclear spin bath[4,54–56].

A quantum dot electron interacts with the nuclear spin of each atom in the quantum dot through the hyperfine interaction (Fig. 6). The conduction states are constructed from atomic *s* orbitals and therefore have a large amplitude at the location of the nuclei. A quantum dot electron spin has an interaction through the contact part of the hyperfine interaction with N ~10^5 nuclear spins (Fig. 6a,b), a 'central spin problem' with a strong mesoscopic character[57]. The number of nuclear spins is too large to be able to use individual nuclear spins as a quantum resource and yet too small for the complete cancellation of the hyperfine interaction. Through the contact part of the hyperfine interaction, each nuclear spin acts on the electron spin via an effective magnetic field (Fig. 6b). For N nuclear spins, the effective magnetic fields tend to cancel, but

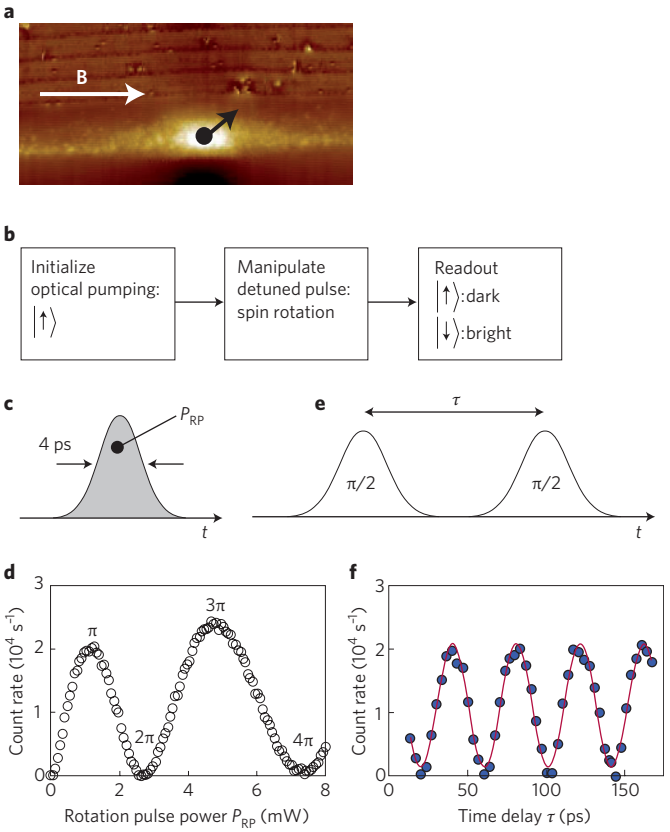

Figure 5 | Ultrafast manipulation of a single electron spin. The experiment of the Yamamoto group[39,40] is presented. **a**, Scanning tunnelling microscope image (as in Fig. 4) showing an electron spin in an in-plane magnetic field (several Tesla). Image size, 80 × 40 nm^2. **b**, An initialize–manipulate–readout scheme is implemented by preparing the spin in the $|\uparrow\rangle$ state with optical pumping (26-ns pulse resonant with the $|\downarrow\rangle \leftrightarrow |\uparrow\downarrow, \Downarrow\rangle$, scheme as in Fig. 4c), manipulating the spin with a 4-ps red-detuned pulse (coupling as in Fig. 3g,h), performing readout with a resonant pulse (as for the initialization pulse), and detecting spontaneous emission at the $|\uparrow\downarrow, \Downarrow\rangle \leftrightarrow |\uparrow\rangle$ energy. In the readout step, $|\downarrow\rangle$ results in the emission of a single photon, $|\uparrow\rangle$ does not. The pulse sequence is repeated many times to accumulate sufficient signal, the readout step of one cycle forming the initialization step of the next. **c**,**d**, The manipulation pulse consists of a single 4-ps pulse whose rotation pulse power (P_{RP}) is gradually increased from zero (**c**), resulting in spin Rabi flopping $|\uparrow\rangle \leftrightarrow |\downarrow\rangle$ as shown in **d**. **e**, Spin manipulation is explored with two 4-ps pulses separated by time τ, P_{RP} is chosen so that each pulse rotates the spin by $\pi/2$. **f**, The readout signal demonstrates Ramsey fringes. Panel **a** courtesy of Paul Koenraad. Panels **d**,**f**, reproduced from ref. 40, © 2010 NPG.

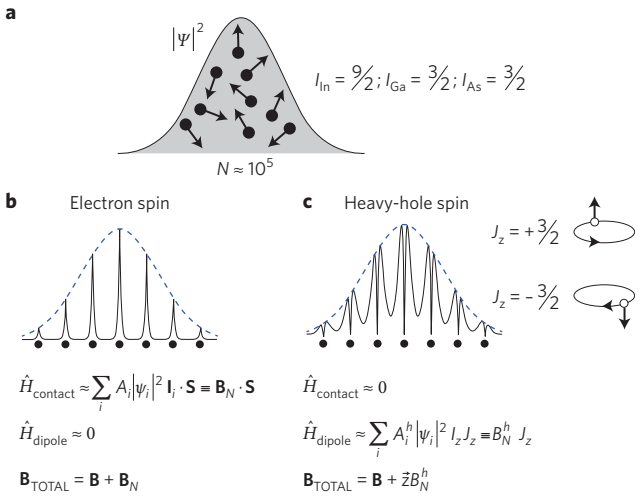

Figure 6 | Hyperfine interaction of an electron spin and a hole spin with the nuclear spins in the host material. a, The electron or hole spin has a wavefunction extending over a few nanometres in all three directions such that it overlaps with about $N \sim 10^5$ atoms in the host material, each atom containing a nucleus with non-zero spin in the case of InGaAs. The nuclear spins are given for the main isotopes. **b**, The conduction state is constructed largely from atomic *s* orbitals, each localized to a unit cell (black line; circles represent the nuclei), modulated by the envelope function that extends over the quantum dot (blue dashed line). The contact part of the hyperfine interaction dominates. In the Hamiltonian H, A_i is the coupling coefficient with nuclear spin i, $\mathbf{I}_i$ is the nuclear spin and ψ_i the electron wavefunction at the location of i. The contact term resembles the interaction of the electron spin $\mathbf{S}$ in a fictitious magnetic field, $\mathbf{B}_N$. The dipole–dipole hyperfine interaction is zero for a pure *s* orbital, and close to zero in practice. **c**, The hole state is constructed largely from atomic *p* orbitals, each localized to a unit cell, such that the wavefunction amplitude is small at the location of each nucleus. This suppresses the contact part of the hyperfine interaction. The dipole–dipole part is non-zero however. A heavy-hole spin has $J_z = \pm 3/2$, corresponding, in a semi-classical interpretation, to a circulating microscopic current clockwise with spin up, or anticlockwise with spin down. The magnetic dipole moment points therefore either along the $+z$ or $-z$ direction such that the dipole–dipole Hamiltonian has an Ising form, $\propto I_z J_z$. Equivalently, the fictitious magnetic field describing the nuclear spins lies solely along the z-direction.

the cancellation is incomplete with the overall field scaling as $1/\sqrt{N}$ (refs 54,55). For an InGaAs quantum dot for instance, the average effective magnetic field (the Overhauser field) is around $B_N \sim 20$ mT. B_N fluctuates in the course of an experiment, leading to dephasing. In a simple view, the components of the contact hyperfine interaction perpendicular to the applied magnetic field represent the electron spin–nuclear spin flip-flop process, exactly the process that is suppressed in a magnetic field, resulting in the large T_1. However, the component of the Overhauser field along the applied field direction cannot be suppressed so simply and in this simple picture, it is this component that results in the fast dephasing. Specifically, in an applied magnetic field B along z, the total field along the applied field direction is $B + B_N^z$ resulting in random changes in the electron spin precession frequency, a dephasing process.

A number of routes are being pursued to limit the dephasing by means of the hyperfine interaction. Polarizing the nuclei optically ('dynamic polarization') is one promising route[57]. Ideally, to suppress the nuclear spin noise, the nuclei should be polarized close to 100%. This has not been achieved so far: nuclear spin polarizations are at present limited to ~50% (ref. 57). However, partial polarization can be combined with feedback control to 'narrow' the distribution[56], that is, reduce the noise in the nuclear spin ensemble[58–61]. In the context of an optical single-spin experiment, this approach has already prolonged T_2^* to about a microsecond[62], and a related idea underpins the spin-mode-locking experiments on an ensemble of quantum dots in which the precession frequencies of an inhomogeneous ensemble of single spins are locked to the same frequency by a feedback provided by the nuclear spins[24,63]. An alternative standpoint is that the nuclear field B_N fluctuates slowly. In transport experiments, gate operations robust to the slow nuclear wanderings have been implemented[64,65]. However, these approaches add a lot of complexity even to the simplest spin operation. A further approach is to reduce the effect of nuclear spin noise by redesigning the spin qubit, in particular seeking a point where the energy separation of the qubit states has no first-order dependence on the magnetic field. This can be achieved by using a quantum dot molecule in the (1,1) state. There are two vertical-tunnel-coupled quantum dots[66], with a single electron in each

quantum dot, defining the qubit with the singlet and triplet states[67]. Recent experiments show that T_2^* can be prolonged to beyond 100 ns with this approach[67].

The time over which spin coherence is irreversibly lost, T_2, has been measured to lie in the microsecond regime[24,40]. Whereas T_2 is considerably longer than T_2^* in the presence of noisy nuclei, T_2 is still considerably shorter than the relaxation time T_1 that is in the millisecond range at modest magnetic fields[46,47]. T_1 is limited by phonons, and when decoherence is also limited by phonons, theory predicts the ideal case, $T_2 = 2T_1$, is achieved[68]. For these reasons, in current experiments it is highly likely that T_2 is also bounded by the nuclear spins. It should be borne in mind that different measurement techniques have different consequences on the nuclear spins, which do not represent a large, memory-less reservoir. Even at small magnetic fields, the nuclei in the quantum dot are largely decoupled from the nuclei in the host material such that the 'environment', the nuclear spin ensemble, is itself small and subject to profound changes[69,70].

Electron spin readout. Using laser techniques, efficient optical spin initialization and spin readout on a single quantum dot pose conflicting requirements. With optical pumping, spin initialization depends on a sizeable diagonal transition rate. Using the same states, spin readout can be carried out by driving ('recycling') one of the vertical transitions for long enough so that a spontaneous emission event is detected. However, the diagonal transitions lead to a back action in the readout process: in an attempt to recycle on a vertical transition alone, spontaneous emission via the diagonal transition can modify the spin state before a photon is detected. Most experiments so far on self-assembled quantum dots have not achieved single-shot readout. Instead, an initialization–manipulation–readout cycle with a short readout time is repeated many times to acquire sufficient signal. The optical readout process can be spin-dependent spontaneous emission[39–41], differential transmission[42,50], Faraday rotation[71] or Kerr rotation[72–74].

Single-shot readout has been achieved however, by increasing the number of available levels with a quantum dot molecule[75] (Fig. 7). In this case, a recycling transition has been discovered: one quantum dot provides the host for the qubit, the other a means to readout the spin.

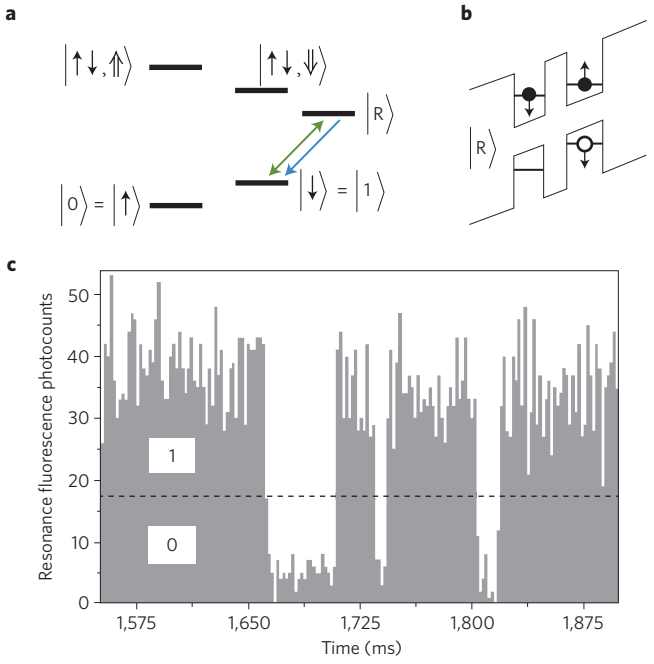

Figure 7 | Single-shot spin readout. a, Idealized readout scheme. An optically active electron spin (magnetic field along z) is available, as in Fig. 3e. Spin readout can be achieved by exploiting a further state, $|R\rangle$, which ideally has an optical coupling to the $|\downarrow\rangle$ state but not to the $|\uparrow\rangle$ state, and only one spontaneous emission channel, $|R\rangle$ back to $|\downarrow\rangle$ (green and blue arrows, respectively). This coupling, $|\downarrow\rangle \leftrightarrow |R\rangle$, represents a recycling transition. Resonance fluorescence intensity from the recycling transition is spin-dependent and represents a close-to-ideal spin measurement. **b**, The spin states $|\uparrow\rangle$, $|\downarrow\rangle$ and the recycling state $|R\rangle$ can be engineered using a quantum dot molecule. The left quantum dot hosts the spin qubit. Absorption in the right quantum dot depends on the spin in the left dot through a tunnel coupling of the electron states. In particular, the molecular state with an electron spin triplet $S_z = -1$ represents a good approximation to the ideal readout state $|R\rangle$. **c**, Resonance fluorescence intensity from the recycling laser is plotted against time (B is a few Tesla) showing spin quantum jumps. High and low signal is associated with states $|1\rangle$ and $|0\rangle$, respectively. Figure reproduced from ref. 75, © 2010 NPG.

The hole spin

A hole can also represent a spin qubit.

Motivations for hole spins. In the optics of an electron spin, the upper state contains a single hole such that the upper-state coherence is determined to some extent by the hole-spin coherence: even for an electron spin, hole-spin coherence plays a role. However, the hole spin may possibly represent a viable spin qubit in its own right[76,77].

In quantum wells where the heavy hole–light hole degeneracy is lifted by quantum confinement and possibly also by non-hydrostatic strain[78,79], the hole-spin coherence is limited by rapid, typically subnanosecond, spin relaxation involving a phonon[80,81]. However, hole-spin relaxation times increase as the temperature decreases as a consequence of hole localization[82,83], strong hints of the potential of quantum dots.

The dephasing of a single electron spin confined to a quantum dot at low magnetic fields arises mainly from noise in the nuclear spins. A hole spin has a quite different hyperfine interaction[84,85] (Fig. 6c). The main point is that the hole states are constructed predominantly from atomic p orbitals, there is one p orbital per atom, with each one having a zero wavefunction amplitude at the location of its host nucleus, such that the hole-spin contact-hyperfine interaction is suppressed (Fig. 6b). The dipole–dipole part of the hyperfine interaction, which is zero for a conduction state constructed from zero angular momentum s orbitals, remains. However, the dipole–dipole hyperfine interaction is highly anisotropic, particularly for a pure heavy-hole state. The heavy-hole states have a magnetic dipole moment along the $\pm z$-direction (Fig. 6c). The coupling of this magnetic dipole to each nuclear spin has an Ising-form (Fig. 6c). Equivalently, a pure heavy-hole spin experiences just the z-component of the noisy Overhauser field. Without an applied magnetic field, this interaction dephases the heavy-hole spin relatively quickly[84,86] but in a reasonably strong in-plane magnetic field, the Ising-like nature of the hyperfine interaction implies that the fluctuations in total magnetic field along the applied field direction are strongly suppressed. A clear prediction for a pure heavy-hole state is that even in the presence of noisy nuclei, the dephasing time T_2^* should increase with increasing in-plane magnetic field[84].

This expectation, that a heavy-hole spin becomes coherent in an in-plane magnetic field even without narrowing the nuclear spin distribution[84], is robust for a pure heavy-hole state. In practice, the hole ground state in a real quantum dot is inevitably an admixture of heavy-hole, light-hole, spin–orbit split-off and conduction Bloch states[87] such that the dipole–dipole part of the hyperfine interaction is no longer purely Ising-like and there is a small contact hyperfine interaction. The challenge is to engineer a nanoconfined close-to-pure heavy-hole spin and then test its spin coherence. Available InGaAs/GaAs quantum dots are an obvious candidate[87].

Materials issues. Control over the hole population in a single quantum dot can be achieved by replacing the n doping in a vertical tunnelling structure with p doping[32,38,88]. The larger effective mass of the hole results in much longer tunnelling times for the hole compared with the electron (for a 25-nm tunnelling barrier for instance, tunnelling times are 10 ns for p doping[32] and 10 ps for n doping[29]). This results in overlapping lines in the bias-dependent photoluminescence and difficulties in fast bias switching, but also in a suppressed co-tunnelling interaction with the Fermi sea[32]. Laser spectroscopy has been established on p-type vertical tunnelling structures[32,38,88]. Quantum dots in samples doped with Be show Fano resonances[88] pointing to an unwanted coupling to continuum states[89]. Lorentzian lineshapes are recovered when Be is replaced with C suggesting that the continuum states in the Be-doped samples are related to Be (which is known to 'float' in the growth process), and that doping with C is clearly superior for these experiments[88]. However, the linewidths of the present p-type samples are at best ~5 μeV, three times larger than for the n-type samples, and the absorption contrast is typically a factor of ten times smaller, features that clearly lead to signal-to-noise difficulties.

An alternative approach is to work with an n-type device in the field ionization regime[90,91]. A large negative bias is applied such that on creation of an electron–hole pair, the electron tunnels out rapidly, leaving the hole behind. The hole survives until it too tunnels out. Tunnelling of both the electron and hole allows the absorption to be detected by a photocurrent, one cycle corresponding to the transfer of one electron through the device[92]. Access to hole-spin physics is also possible with doping: a δ-doping layer has been used to occupy an ensemble of quantum dots with a single hole on average[25].

Hole spin initialization. Optical pumping has been used to initialize the hole spin[32]. The hole-spin optical-pumping scheme was found to work even at zero applied magnetic field when the two hole spin states are degenerate: with either σ^+ or σ^- laser polarization the ΔT-signal disappears[32] (Fig. 8a–c). The interpretation is that the exciton states are coupled by the hyperfine interaction (Fig. 3f) allowing the hole spin to be pumped into $|\Uparrow\rangle_z$ or $|\Downarrow\rangle_z$ states with σ^+ or σ^- excitation, respectively: the hole is shielded from the laser only by its spin and not by an energy detuning. With two same-wavelength lasers, one σ^+-polarized and the other σ^--polarized, the ΔT-signal reappears (Fig. 8d). Success at $B = 0$ depends not only on very clean selection rules and slow hole-spin relaxation but also on close-to-zero coupling of the $|\Uparrow\rangle_z$ and $|\Downarrow\rangle_z$ states by the Overhauser field. This experiment demonstrates the Ising nature of the hole spin hyperfine interaction. Not all the quantum dots in this particular sample show such clear spin pumping at $B = 0$: the reason for this is not known but is probably related to different heavy hole–light hole admixtures. The ΔT-signal, suppressed at $B = 0$, gradually reappears as B is increased[32]. This can be understood quantitatively with a model that assumes that the diagonal transition rates are dominated by the Overhauser field experienced by the electron spin, and that the hole spin relaxation time T_1 is B-independent[32]. Notably, $B \simeq 3$ T is required to recover the full single laser ΔT-signal at which point the diagonal transition rate is extremely small pointing to a large T_1, in this case about a millisecond.

T_1 has also been measured on an ensemble of hole spins by initializing the hole spins in the field ionization regime and after a wait time, applying a forward bias pulse such that two electrons are added to each dot[93]. The resulting polarization of the emission is a measure of the remaining hole spin. T_1 is revealed to be a few hundred microseconds at $B = 1.5$ T, reducing to about 10 μs at high magnetic fields, $B = 12$ T. As for the electron spin, the hole spin T_1 exhibits a T^{-1}-dependence, pointing to the dominance of a phonon-related relaxation mechanism. Furthermore, both experiments suggest that T_1 has at most a weak magnetic field dependence at low fields[32,93]. This too is consistent with a phonon-related mechanism: for a hole spin at low field, theory suggests that the one-phonon process is overtaken by a two-phonon process, resulting in a weak magnetic field dependence[94,95].

Hole spin coherence. Coherent population trapping on a single hole in a quantum dot provides evidence for a coherent hole spin[38]. In a modest in-plane magnetic field, there is a clear dip in the probe absorption spectrum (measured in this case with differential reflectivity, ΔR) in the presence of the pump (Fig. 8e,f). The 'visibility' of this quantum interference (that is, the depth of the dip) is sensitive to the hole spin coherence time[96]; equivalently, the signal in the dip measures the extent to which the dark state (Fig. 3g) is admixed with the other two eigenstates of the Λ-system by the environment. The experiment sets a lower bound on $T_2^\star$ of about 100 ns. An equivalently long $T_2^\star$ time has also been reported on a hole spin ensemble, measuring the coherence via the noise in a Faraday rotation experiment[25]. Pulsed-laser experiments have recently demonstrated ultrafast hole-spin rotations both in a single quantum dot[41] and in a single quantum dot molecule[42], the latter experiment also demonstrated a coherent dot–dot coupling. In these experiments, $T_2^\star$ is smaller than in the coherent population trapping and spin noise experiments. Remarkably however, the hole spin decoherence time T_2 turns out to be similar to the electron spin decoherence time[41], which is a few microseconds.

The coupling coefficient of the dipole–dipole part of the hole spin hyperfine interaction has been measured by dynamically polarizing the nuclear spins in the z-direction and measuring the changes to the electron and hole Zeeman energies, that is, the Overhauser fields. For both InGaAs/GaAs (ref. 97) and InP/GaInP quantum dots[98], the hole Zeeman energy shift is approximately −10% of that of the electron Zeeman energy. This is consistent with estimates of the heavy-hole dipole–dipole to electron contact hyperfine interactions[84]. However, the full topology of the hole hyperfine interaction and its dependence on the make-up of the hole state has not yet been determined.

A further significant feature concerns the electric field dependence of the hole g-factor[99]. Although this may be useful for all-electrical control of the hole spin[100], it leads to a sensitivity of the hole spin coherence to charge noise, and how these sources of noise play out and can be controlled is unknown at present.

Conclusions and outlook

Single self-assembled quantum dots are now established as quasi-atoms. In some respects, the optical properties mimic those of real atoms very closely. In other respects however, the optical properties reflect the complex solid-state environment. This interplay has driven a lot of the research in this area. Crucially, the flexibility of semiconductor devices can be used to engineer the system so that either the atom-like properties or the complex solid-state properties dominate. For instance, a quantum dot can be strongly coupled to a Fermi sea or to the nuclear spins, allowing some old problems in solid-state physics (the Kondo effect[101–103] and central spin problem[57]) to be revisited profitably. Alternatively, a spin state can already be decoupled sufficiently from the main sources of noise to achieve long spin-relaxation times. All-optical techniques for high-fidelity spin initialization, fast spin rotations and single-shot readout now exist. In parallel, huge progress has been made in engineering the photonic states with which a single quantum dot interacts[15,104]. Examples include the design and realization of low-volume, high-Q microcavities[104] and one-dimensional waveguides[15].

The main challenge is to extend the spin coherence while maintaining the capability of fast, high-fidelity spin initialization, manipulation and readout. Promising candidates at present are a single electron spin with dynamically cooled nuclei; a single hole spin; and a singlet–triplet qubit in a quantum dot molecule. A realistic goal is to engineer a robust $T_2^\star$ time on the microsecond scale

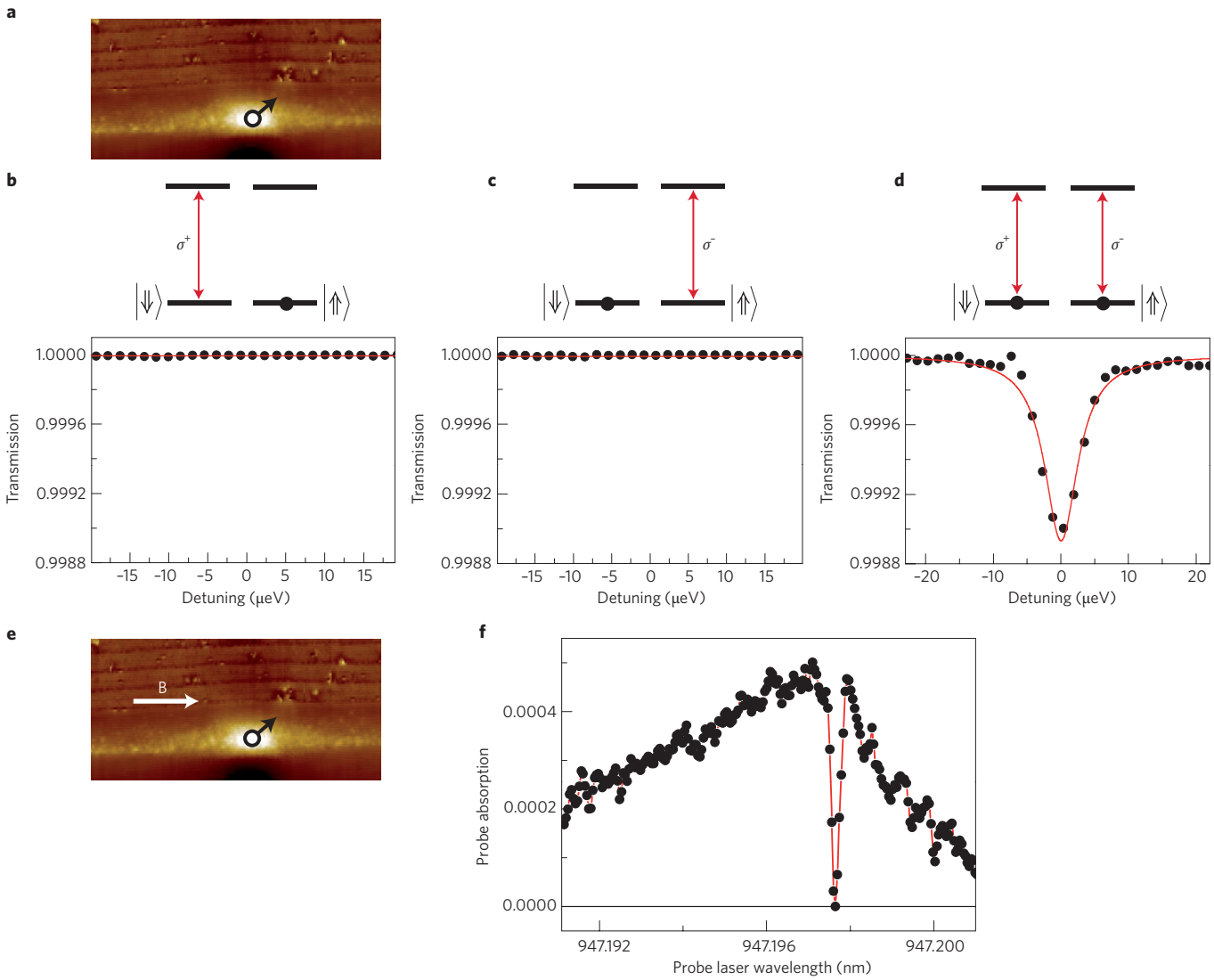

Figure 8 | Hole spin initialization and manipulation. a, A single hole confined to a self-assembled quantum dot is shown in the scanning tunnelling microscopy image, 80 × 40 nm^2. **b**–**d**, Showing spin pumping at zero magnetic field. The transmission dip with pure σ^+-excitation disappears as the hole spin is pumped into the $|\Uparrow\rangle$ state (**b**). The transmission dip with pure σ^--excitation disappears as the hole spin is pumped into the $|\Downarrow\rangle$ state (**c**). The transmission dip reappears with simultaneous σ^+- and σ^--excitation (equivalently a single laser with linear polarization), each laser acting as the re-pump laser for the other[32] (**d**). The schematics (top) show the levels and populations relevant to the experimental data (bottom). **e**, A self-assembled quantum dot at 4.2 K with single hole in an in-plane magnetic field. Image size, 80 × 40 nm^2. **f**, Experimental coherent population trapping (CPT) data with $B = 2.3$ T along the x-direction, $\hbar\Omega_1 = 0.75$ μeV, $\hbar\Omega_2 = 0.34$ μeV. A clear dip is revealed in the probe absorption spectrum: the dip signifies that the hole spin is projected into a dark state at the two-photon resonance (CPT, Fig. 3g), the high visibility of the dip points to a coherent hole spin[38]. Panel **a** courtesy of Paul Koenraad. Figure reproduced with permission from: **b**–**d**, ref. 32, © 2008 NPG; **f**, ref. 38, © 2009 AAAS.

for a fully optical spin qubit. These efforts demand a better understanding of both charge and spin noise in semiconductor devices. Furthermore, in the spirit of 'bandstructure engineering' that drove the development of high-speed semiconductor transistors and lasers, 'quantum engineering' is required to combine spin coherence, an enhanced light–matter coupling[105] and fast electrical switching[33,106]. To go beyond the one qubit level and to create multiqubit entangled states, control of the photonic states is crucial: powerful paradigms involve coupling separate qubits through a common microcavity mode[107]; or by creating entanglements between remote spins using photon–photon interference. The wide disparity of quantum dots from one to the next represents a challenge of course. A possible approach involves preselecting quantum dots from an ensemble that by chance happen to have similar properties, and then carrying out *in situ* fine tuning, either with an electric field or with an applied strain. Some further materials development is also important: a spin/photon interface in the telecommunications band does not exist yet for instance; and attempts at building hybrid quantum systems, coupling quantum dots to superconducting systems, atomic ensembles[108] or trapped ions for best-of-both-worlds hybrid technologies are at present in their infancy.

Received 5 April 2012; accepted 29 January 2013; published 22 May 2013

References

1. Loss, D. & DiVincenzo, D. P. Quantum computation with quantum dots. *Phys. Rev. A* **57,** 120–126 (1998).
2. Khaetskii, A. V. & Nazarov, Y. V. Spin-flip transitions between Zeeman sublevels in semiconductor quantum dots. *Phys. Rev. B* **64,** 125316 (2001).
3. Balasubramanian, G. *et al.* Ultralong spin coherence time in isotopically engineered diamond. *Nature Mater.* **8,** 383–387 (2009).

4. Fischer, J. & Loss, D. Dealing with decoherence. *Science* **324,** 1277–1278 (2009).
5. Hanson, R., Kouwenhoven, L. P., Petta, J. R., Tarucha, S. & Vandersypen, L. M. K. Spins in few-electron quantum dots. *Rev. Mod. Phys.* **79,** 1217–1265 (2007).
6. Petta, J. R. *et al.* Coherent manipulation of coupled electron spins in semiconductor quantum dots. *Science* **309,** 2180–2184 (2005).
7. Liu, R. B., Yao, W. & Sham, L. J. Quantum computing by optical control of electron spins. *Adv. Phys.* **59,** 703–802 (2010).
8. Leonard, D., Pond, K. & Petroff, P. M. Critical layer thickness for self-assembled InAs islands on GaAs. *Phys. Rev. B* **50,** 11687–11692 (1994).
9. Mlinar, V. *et al.* Structure of quantum dots as seen by excitonic spectroscopy versus structural characterization: Using theory to close the loop. *Phys. Rev. B* **80,** 165425 (2009).
10. Zrenner, A. A close look on single quantum dots. *J. Chem. Phys.* **112,** 7790–7798 (2000).
11. Garcia, J. M., Mankad, T., Holtz, P. O., Wellman, P. J. & Petroff, P. M. Electronic states tuning of InAs self-assembled quantum dots. *Appl. Phys. Lett.* **72,** 3172–3174 (1998).
12. Langbein, W. *et al.* Control of fine-structure splitting and biexciton binding in $In_xGa_{1-x}As$ quantum dots by annealing. *Phys. Rev. B* **69,** 161301 (2004).
13. Dalgarno, P. A. *et al.* Coulomb interactions in single charged self-assembled quantum dots: Radiative lifetime and recombination energy. *Phys. Rev. B* **77,** 245311 (2008).
14. Karrai, K. & Warburton, R. J. Optical transmission and reflection spectroscopy of single quantum dots. *Superlattices and Microstructures* **33,** 311–337 (2003).
15. Claudon, J. *et al.* A highly efficient single-photon source based on a quantum dot in a photonic nanowire. *Nature Photon.* **4,** 174–177 (2010).
16. Hogele, A. *et al.* Voltage-controlled optics of a quantum dot. *Phys. Rev. Lett.* **93,** 217401 (2004).
17. Muller, A. *et al.* Resonance fluorescence from a coherently driven semiconductor quantum dot in a cavity. *Phys. Rev. Lett.* **99,** 187402 (2007).
18. Vamivakas, A. N., Zhao, Y., Lu, C. Y. & Atatuere, M. Spin-resolved quantum-dot resonance fluorescence. *Nature Phys.* **5,** 198–202 (2009).
19. Yilmaz, S. T., Fallahi, P. & Imamoglu, A. Quantum-dot-spin single-photon interface. *Phys. Rev. Lett.* **105,** 033601 (2010).
20. Kroner, M. *et al.* Resonant saturation laser spectroscopy of a single self-assembled quantum dot. *Physica E* **40,** 1994–1996 (2008).
21. Kroner, M. *et al.* Rabi splitting and ac-Stark shift of a charged exciton. *Appl. Phys. Lett.* **92,** 031108 (2008).
22. Houel, J. *et al.* Probing single-charge fluctuations at a GaAs/AlAs interface using laser spectroscopy on a nearby InGaAs quantum dot. *Phys. Rev. Lett.* **108,** 107401 (2012).
23. Ramsay, A. J. *et al.* Damping of exciton Rabi rotations by acoustic phonons in optically excited InGaAs/GaAs quantum dots. *Phys. Rev. Lett.* **104,** 017402 (2010).
24. Greilich, A. *et al.* Mode locking of electron spin coherences in singly charged quantum dots. *Science* **313,** 341–345 (2006).
25. Crooker, S. A. *et al.* Spin noise of electrons and holes in self-assembled quantum dots. *Phys. Rev. Lett.* **104,** 036601 (2010).
26. Drexler, H., Leonard, D., Hansen, W., Kotthaus, J. P. & Petroff, P. M. Spectroscopy of quantum levels in charge-tunable InGaAs quantum dots. *Phys. Rev. Lett.* **73,** 2252–2255 (1994).
27. Warburton, R. J. *et al.* Optical emission from a charge-tunable quantum ring. *Nature* **405,** 926–929 (2000).
28. Seidl, S. *et al.* Absorption and photoluminescence spectroscopy on a single self-assembled charge-tunable quantum dot. *Phys. Rev. B* **72,** 195339 (2005).
29. Smith, J. M. *et al.* Voltage control of the spin dynamics of an exciton in a semiconductor quantum dot. *Phys. Rev. Lett.* **94,** 197402 (2005).
30. Atature, M. *et al.* Quantum-dot spin-state preparation with near-unity fidelity. *Science* **312,** 551–553 (2006).
31. Dreiser, J. *et al.* Optical investigations of quantum dot spin dynamics as a function of external electric and magnetic fields. *Phys. Rev. B* **77,** 075317 (2008).
32. Gerardot, B. D. *et al.* Optical pumping of a single hole spin in a quantum dot. *Nature* **451,** 441–444 (2008).
33. McFarlane, J. *et al.* Gigahertz bandwidth electrical control over a dark exciton-based memory bit in a single quantum dot. *Appl. Phys. Lett.* **94,** 093113 (2009).
34. Hogele, A. *et al.* Spin-selective optical absorption of singly charged excitons in a quantum dot. *Appl. Phys. Lett.* **86,** 221905 (2005).
35. Belhadj, T. *et al.* Impact of heavy hole-light hole coupling on optical selection rules in GaAs quantum dots. *Appl. Phys. Lett.* **97,** 051111 (2010).
36. Fleischhauer, M., Imamoglu, A. & Marangos, J. P. Electromagnetically induced transparency: Optics in coherent media. *Rev. Mod. Phys.* **77,** 633–673 (2005).
37. Xu, X. *et al.* Coherent population trapping of an electron spin in a single negatively charged quantum dot. *Nature Phys.* **4,** 692–695 (2008).
38. Brunner, D. *et al.* A coherent single-hole spin in a semiconductor. *Science* **325,** 70–72 (2009).
39. Press, D., Ladd, T. D., Zhang, B. & Yamamoto, Y. Complete quantum control of a single quantum dot spin using ultrafast optical pulses. *Nature* **456,** 218–221 (2008).
40. Press, D. *et al.* Ultrafast optical spin echo in a single quantum dot. *Nature Photon.* **4,** 367–370 (2010).
41. De Greve, K. *et al.* Ultrafast coherent control and suppressed nuclear feedback of a single quantum dot hole qubit. *Nature Phys.* **7,** 872–878 (2011).
42. Greilich, A., Carter, S. G., Kim, D., Bracker, A. S. & Gammon, D. Optical control of one and two hole spins in interacting quantum dots. *Nature Photon.* **5,** 703–709 (2011).
43. Kroner, M. *et al.* Resonant two-color high-resolution spectroscopy of a negatively charged exciton in a self-assembled quantum dot. *Phys. Rev. B* **78,** 075429 (2008).
44. Braun, P. F. *et al.* Direct observation of the electron spin relaxation induced by nuclei in quantum dots. *Phys. Rev. Lett.* **94,** 116601 (2005).
45. Amasha, S. *et al.* Electrical control of spin relaxation in a quantum dot. *Phys. Rev. Lett.* **100,** 046803 (2008).
46. Kroutvar, M. *et al.* Optically programmable electron spin memory using semiconductor quantum dots. *Nature* **432,** 81–84 (2004).
47. Lu, C-Y. *et al.* Direct measurement of spin dynamics in InAs/GaAs quantum dots using time-resolved resonance fluorescence. *Phys. Rev. B* **81,** 035332 (2010).
48. Xu, X. *et al.* Fast spin state initialization in a singly charged InAs-GaAs quantum dot by optical cooling. *Phys. Rev. Lett.* **99,** 097401 (2007).
49. Koppens, F. H. L. *et al.* Driven coherent oscillations of a single electron spin in a quantum dot. *Nature* **442,** 766–771 (2006).
50. Kroner, M. *et al.* Optical detection of single-electron spin resonance in a quantum dot. *Phys. Rev. Lett.* **100,** 156803 (2008).
51. Kastler, A. Optical methods of atomic orientation and of magnetic resonance. *J. Opt. Soc. Am.* **47,** 460–465 (1957).
52. Golovach, V. N., Borhani, M. & Loss, D. Electric-dipole-induced spin resonance in quantum dots. *Phys. Rev. B* **74,** 165319 (2006).
53. Nowack, K. C., Koppens, F. H. L., Nazarov, Y. V. & Vandersypen, L. M. K. Coherent control of a single electron spin with electric fields. *Science* **318,** 1430–1433 (2007).
54. Merkulov, I. A., Efros, A. L. & Rosen, M. Electron spin relaxation by nuclei in semiconductor quantum dots. *Phys. Rev. B* **65,** 205309 (2002).
55. Khaetskii, A. V., Loss, D. & Glazman, L. Electron spin decoherence in quantum dots due to interaction with n uclei. *Phys. Rev. Lett.* **88,** 186802 (2002).
56. Coish, W. A. & Loss, D. Hyperfine interaction in a quantum dot: Non-Markovian electron spin dynamics. *Phys. Rev. B* **70,** 195340 (2004).
57. Urbaszek, B. *et al.* Nuclear spin physics in quantum dots: an optical investigation. *Rev. Mod. Phys.* **85,** 79–133 (2013).
58. Latta, C. *et al.* Confluence of resonant laser excitation and bidirectional quantum-dot nuclear-spin polarization. *Nature Phys.* **5,** 758–763 (2009).
59. Vink, I. T. *et al.* Locking electron spins into magnetic resonance by electron–nuclear feedback. *Nature Phys.* **5,** 764–768 (2009).
60. Bluhm, H., Foletti, S., Mahalu, D., Umansky, V. & Yacoby, A. Enhancing the coherence of a spin qubit by operating it as a feedback loop that controls its nuclear spin bath. *Phys. Rev. Lett.* **105,** 216803 (2010).
61. Kloeffel, C. *et al.* Controlling the interaction of electron and nuclear spins in a tunnel-coupled quantum dot. *Phys. Rev. Lett.* **106,** 046802 (2011).
62. Xu, X. *et al.* Optically controlled locking of the nuclear field via coherent dark-state spectroscopy. *Nature* **459,** 1105–1109 (2009).
63. Greilich, A. *et al.* Nuclei-induced frequency focusing of electron spin coherence. *Science* **317,** 1896–1899 (2007).
64. Barthel, C., Medford, J., Marcus, C. M., Hanson, M. P. & Gossard, A. C. Interlaced dynamical decoupling and coherent operation of a singlet-triplet qubit. *Phys. Rev. Lett.* **105,** 266808 (2010).
65. Bluhm, H. *et al.* Dephasing time of GaAs electron-spin qubits coupled to a nuclear bath exceeding 200 μs. *Nature Phys.* **7,** 109–113 (2011).
66. Stinaff, E. A. *et al.* Optical signatures of coupled quantum dots. *Science* **311,** 636–639 (2006).
67. Weiss, K. M., Elzerman, J. M., Delley, Y. L., Miguel-Sanchez, J. & Imamoglu, A. Coherent two- electron spin qubits in an optically active pair of coupled InGaAs quantum dots. *Phys. Rev. Lett.* **109,** 107401 (2012).
68. Golovach, V. N., Khaetskii, A. & Loss, D. Phonon-induced decay of the electron spin in quantum dots. *Phys. Rev. Lett.* **93,** 016601 (2004).
69. Maletinsky, P., Badolato, A. & Imamoglu, A. Dynamics of quantum dot nuclear spin polarization controlled by a single electron. *Phys. Rev. Lett.* **99,** 056804 (2007).
70. Latta, C., Srivastava, A. & Imamoglu, A. Hyperfine interaction-dominated dynamics of nuclear spins in self-assembled InGaAs quantum dots. *Phys. Rev. Lett.* **107,** 167401 (2011).
71. Atatuere, M., Dreiser, J., Badolato, A. & Imamoglu, A. Observation of Faraday rotation from a single confined spin. *Nature Phys.* **3,** 101–105 (2007).

72. Berezovsky, J. *et al.* Nondestructive optical measurements of a single electron spin in a quantum dot. *Science* **314,** 1916–1920 (2006).
73. Mikkelsen, M. H., Berezovsky, J., Stoltz, N. G., Coldren, L. A. & Awschalom, D. D. Optically detected coherent spin dynamics of a single electron in a quantum dot. *Nature Phys.* **3,** 770–773 (2007).
74. Berezovsky, J., Mikkelsen, M. H., Stoltz, N. G., Coldren, L. A. & Awschalom, D. D. Picosecond coherent optical manipulation of a single electron spin in a quantum dot. *Science* **320,** 349–352 (2008).
75. Vamivakas, A. N. *et al.* Observation of spin-dependent quantum jumps via quantum dot resonance fluorescence. *Nature* **467,** 297–300 (2010).
76. Bulaev, D. V. & Loss, D. Spin relaxation and decoherence of holes in quantum dots. *Phys. Rev. Lett.* **95,** 076805 (2005).
77. Bulaev, D. V. & Loss, D. Electric dipole spin resonance for heavy holes in quantum dots. *Phys. Rev. Lett.* **98,** 097202 (2007).
78. Warburton, R. J. *et al.* Strain reconstruction of the valence band in $Ga_{1-x}In_xSb$ GaSb quantum-wells. *Surf. Sci.* **228,** 270–274 (1990).
79. Martin, R. W. *et al.* Two-dimensional spin confinement in strained-layer quantum wells. *Phys. Rev. B* **42,** 9237–9240 (1990).
80. Damen, T. C., Vina, L., Cunningham, J. E., Shah, J. & Sham, L. J. Subpicosecond spin relaxation dynamics of excitons and free-carriers in GaAs quantum-wells. *Phys. Rev. Lett.* **67,** 3432–3435 (1991).
81. Marie, X. *et al.* Hole spin quantum beats in quantum-well structures. *Phys. Rev. B* **60,** 5811–5817 (1999).
82. Syperek, M. *et al.* Spin coherence of holes in GaAs/(Al,Ga)As quantum wells. *Phys. Rev. Lett.* **99,** 187401 (2007).
83. Fokina, L. V. *et al.* Spin dynamics of electrons and holes in InGaAs/GaAs quantum wells at millikelvin temperatures. *Phys. Rev. B* **81,** 195304 (2010).
84. Fischer, J., Coish, W. A., Bulaev, D. V. & Loss, D. Spin decoherence of a heavy hole coupled to nuclear spins in a quantum dot. *Phys. Rev. B* **78,** 155329 (2008).
85. Testelin, C., Bernardot, F., Eble, B. & Chamarro, M. Hole-spin dephasing time associated with hyperfine interaction in quantum dots. *Phys. Rev. B* **79,** 195440 (2009).
86. Eble, B. *et al.* Hole-nuclear spin interaction in quantum dots. *Phys. Rev. Lett.* **102,** 146601 (2009).
87. Bester, G., Nair, S. & Zunger, A. Pseudopotential calculation of the excitonic fine structure of millionatom self-assembled $In_{1-x}Ga_xAs$/GaAs quantum dots. *Phys. Rev. B* **67,** 161306 (2003).
88. Gerardot, B. D. *et al.* Laser spectroscopy of individual quantum dots charged with a single hole. *Appl. Phys. Lett.* **99,** 243112 (2011).
89. Kroner, M. *et al.* The nonlinear Fano effect. *Nature* **451,** 311–314 (2008).
90. Ramsay, A. J. *et al.* Fast optical preparation, control, and readout of a single quantum dot spin. *Phys. Rev. Lett.* **100,** 197401 (2008).
91. Godden, T. M., Boyle, S. J., Ramsay, A. J., Fox, A. M. & Skolnick, M. S. Fast high fidelity hole spin initialization in a single InGaAs quantum dot. *Appl. Phys. Lett.* **97,** 061113 (2010).
92. Zrenner, A. *et al.* Coherent properties of a two-level system based on a quantum-dot photodiode. *Nature* **418,** 612–614 (2002).
93. Heiss, D. *et al.* Observation of extremely slow hole spin relaxation in self-assembled quantum dots. *Phys. Rev. B* **76,** 241306 (2007).
94. Trif, M., Simon, P. & Loss, D. Relaxation of hole spins in quantum dots via two-phonon processes. *Phys. Rev. Lett.* **103,** 106601 (2009).
95. Wei, H., Gong, M., Guo, G. C. & He, L. Atomistic pseudopotential theory of spin relaxation in selfassembled $In_{1-x}Ga_xAs$/GaAs quantum dots at zero magnetic field. *Phys. Rev. B* **85,** 045317 (2012).
96. Imamoglu, A. Coherent population trapping in a single-hole-charged quantum dot. *Phys. Stat. Sol. (b)* **243,** 3725–3729 (2006).
97. Fallahi, P., Yilmaz, S. T. & Imamoglu, A. Measurement of a heavy-hole hyperfine interaction in InGaAs quantum dots using resonance fluorescence. *Phys. Rev. Lett.* **105,** 257402 (2010).
98. Chekhovich, E. A., Krysa, A. B., Skolnick, M. S. & Tartakovskii, A. I. Direct measurement of the hole-nuclear spin interaction in single InP/GaInP quantum dots using photoluminescence spectroscopy. *Phys. Rev. Lett.* **106,** 027402 (2011).
99. Jovanov, V. *et al.* Observation and explanation of strong electrically tunable exciton *g* factors in composition engineered In(Ga)As quantum dots. *Phys. Rev. B* **83,** 161303 (2011).
100. Pingenot, J., Pryor, C. E. & Flatté, M. E. Method for full Bloch sphere control of a localized spin via a single electrical gate. *Appl. Phys. Lett.* **92,** 222502 (2008).
101. Govorov, A. O., Karrai, K. & Warburton, R. J. Kondo excitons in self-assembled quantum dots. *Phys. Rev. B* **67,** 241307 (2003).
102. Dalgarno, P. A. *et al.* Optically induced hybridization of a quantum dot state with a filled continuum. *Phys. Rev. Lett.* **100,** 176801 (2008).
103. Latta, C. *et al.* Quantum quench of Kondo correlations in optical absorption. *Nature* **474,** 627–630 (2011).
104. Vahala, K. J. Optical microcavities. *Nature* **424,** 839–846 (2003).
105. Rakher, M. T., Stoltz, N. G., Coldren, L. A., Petroff, P. M. & Bouwmeester, D. Externally mode-matched cavity quantum electrodynamics with charge-tunable quantum dots. *Phys. Rev. Lett.* **102,** 097403 (2009).
106. Kim, D., Carter, S. G., Greilich, A., Bracker, A. S. & Gammon, D. Ultrafast optical control of entanglement between two quantum-dot spins. *Nature Phys.* **7,** 223–229 (2011).
107. Imamoglu, A. *et al.* Quantum information processing using quantum dot spins and cavity QED. *Phys. Rev. Lett.* **83,** 4204–4207 (1999).
108. Akopian, N., Wang, L., Rastelli, A., Schmidt, O. G. & Zwiller, V. Hybrid semiconductor-atomic interface: slowing down single photons from a quantum dot. *Nature Photon.* **5,** 230–233 (2011).

Acknowledgements

Heartfelt thanks go to my two main collaborators K. Karrai and P. M. Petroff. R. J. W. thanks C. Kloeffel and A. Ludwig for reading the manuscript critically; A. Kuhlmann, J. Houel and A. Ludwig for providing unpublished data; and financial support from the Swiss National Science Foundation and NCCR Quantum Science and Technology.

Additional information

Reprints and permissions information is available online at www.nature.com/reprints. Correspondence should be addressed to R.J.W.

Competing financial interests

The authors declare no competing financial interests.